

Probing the Nature of High- z Short GRB 090426 with Its Early Optical and X-ray Afterglows

Li-ping Xin^{1*}, En-wei Liang^{2†}, Jian-yan Wei¹, Bing Zhang³, Hou-jun Lv², Wei-kang Zheng⁴, Yuji Urata⁵, Myungshin Im⁶, Jing Wang¹, Yu-lei Qiu¹, Jin-song Deng¹, Kui-yun Huang⁵, Jing-yao Hu¹, Yiseul Jeon⁶, Hua-li Li¹ and Xu-hui Han¹

¹ National Astronomical Observatories, Chinese Academy of Sciences, Beijing 100012, China.

² Department of Physics, Guangxi University, Guangxi 530004, China.

³ Department of Physics and Astronomy, University of Nevada, Las Vegas, Nv 89154, USA.

⁴ Department of Physics, University of Michigan, Ann Arbor, MI 48109, USA.

⁵ Institute of Astronomy and Astrophysics, Academia Sinica, P.O. Box 23-141, Taipei 106, Taiwan.

⁶ Center for the Exploration of the Origin of the Universe, Department of Physics & Astronomy, FPRD, Seoul National University, Shillim-dong, San 56-1, Kwanak-gu, Seoul, Korea.

Accepted Received: Revision 1

ABSTRACT

Swift GRB 090426 is a short duration burst ($T_{90} \sim 1.28$ s in the observer frame, and $T_{90} \sim 0.33$ s in the burst frame at $z = 2.609$). Its host galaxy properties and some γ -ray related correlations are analogous to those seen in long duration GRBs, which are believed to be of a massive-star origin (Type II GRBs). We present the results of its early optical observations with the 0.8-m TNT telescope at Xinglong observatory, and the 1-m LOAO telescope at Mt. Lemmon Optical Astronomy Observatory in Arizona. Our well-sampled optical afterglow lightcurve covers from ~ 90 seconds to $\sim 10^4$ seconds post the GRB trigger. It shows two shallow decay episodes that are likely due to energy injection, which end at ~ 230 seconds and ~ 7100 seconds, respectively. The decay slopes post the injection phases are consistent with each other ($\alpha \simeq 1.22$). The X-ray afterglow lightcurve seems to trace the optical one, although the second energy injection phase was missed due to the orbital constraints of the *Swift* satellite. The X-ray spectral index is $\beta_X \sim 1.0$ without temporal evolution. Its decay slope is consistent with the prediction of the forward shock model. Both X-ray and optical emission is consistent with being in the same spectral regime above the cooling frequency (ν_c). The fact that ν_c is below the optical band from the very early epoch of the observation poses a constraint to the burst environment, which is similar to that of a typical Type II GRB. We therefore suggest that death of a massive star is the possible progenitor of this short burst.

Key words: gamma rays: bursts (individual: GRB 090426)—gamma rays: observations.

1 INTRODUCTION

Cosmic gamma-ray bursts (GRBs) are classified into two classes with a separation at the observed burst duration of $T_{90} \sim 2$ seconds based on CGRO/BATSE observations (Kouveliotou et al. 1993). Afterglow and host galaxy properties of long GRBs, especially the detections of several

long GRB-supernova associations (e.g. Galama et al. 1998; Hjorth et al. 2003; Soderberg et al. 2004; Campana et al. 2006), suggest that they are mostly likely related to deaths of massive stars. The “collapsar” model has been widely recognized as the standard scenario for long GRBs (Woosley 1993; Paczyński 1998; Zhang & Mészáros 2004; Piran 2004; Woosley & Bloom 2006). In the *Swift* era, the afterglows and host galaxies of some short GRBs were detected and identified (Gehrels et al. 2005; Villaseñor et al. 2005; Fox et al. 2005; Berger et al. 2005; McGlynn et al. 2008). Some short

* email: xlp@bao.ac.cn

† email: lew@gxu.edu.cn

GRBs were found to be associated with nearby early-type galaxies with little star formation. Some others are located in late-type star forming galaxies (e.g. Fox et al. 2005; Fong et al. 2010), some of which are at high redshifts (Levan et al. 2006; Berger et al. 2007). No short-duration GRB was found to be associated with a supernova (Kann et al. 2008; Zhang et al. 2009, and references therein). All these seem to favor the idea that short GRBs are from mergers of two compact stellar objects (Eichler et al. 1989; Narayan et al. 1992).

Swift observations revealed that the long vs. short GRB classification scheme does not always match the physical classification scheme Type II (collapses of massive stars) vs. Type I (mergers of compact stars) (Zhang et al. 2007a; Kann et al. 2007, 2008; Zhang et al. 2009; Lv et al. 2010). Some convincing Type I GRBs have long, soft “extended emission” (Barthelmy et al. 2005; Norris et al. 2006; Lin et al. 2008; Zhang et al. 2009; Perley et al. 2009), making their T_{90} “long”. The non-detection of any supernovae associated with the nearby long GRBs 060614 and 060505 (Gehrels et al. 2006; Gal-Yam et al. 2006; Fynbo et al. 2006) casted doubts on the Type II origin for these long GRBs. Some long GRBs have rest-frame durations shorter than 2 seconds (Levan et al. 2007). Observations of two intrinsically short-duration, high- z GRBs 080913 ($z = 6.7$; Greiner et al. 2009a) and 090423 ($z = 8.3$; Tanvir et al. 2009; Salvaterra et al. 2009) suggest that they share a lot of common properties with long GRBs, and most likely have a massive star progenitor (Zhang et al. 2009; Lin et al. 2009; Levesque et al. 2010a; Belczynski et al. 2010). Zhang et al. (2009) and Virgili et al. (2009) suggested that some (or even most) short duration GRBs are probably not produced via compact star mergers (Type I), but are likely related to massive stars (Type II). Based on the observed gamma-ray energy and peak energy of the νf_ν spectrum of prompt gamma-ray emission, Lv et al. (2010) defined a parameter $\varepsilon \equiv E_{\text{iso}}/E_{p,z}^{1.7}$, and proposed a new empirical classification scheme that is found to better match the physically-motivated Type II/I classification scheme. They showed that the typical Type II GRBs are in the high- ε group, in contrast to the typical type I GRBs, which belong to the low- ε group.

Another striking case that poses a challenge to the conventional long vs. short GRB classification scheme is GRB 090426. This burst has an observed $T_{90} = 1.29 \pm 0.09$ seconds in the *Swift* BAT band (Sato et al. 2009), corresponding to a burst rest-frame duration of 0.33 s at redshift $z = 2.609$ (Levesque et al. 2010a). Phenomenologically, it is unambiguously within the range of classical short-type GRBs in both the observer frame and the burst rest frame. On the other hand, both the host galaxy properties (Levesque et al. 2010a) and the spectral energy properties (Antonelli et al. 2009) suggest that it is mostly likely a Type II GRB, i.e., related to core collapse of a massive star. With the new classification method proposed by Lv et al. (2010), this event is also well classified into the high- ε group, which is where all known Type II GRBs belongs to.

Multi-wavelength afterglows are essential for revealing the burst environment, and hence can serve as a probe of the GRB progenitor. In this paper, we report our observations of the early optical afterglows for GRB 090426 using the TNT telescope at Xinglong Observatory and the LOAO telescope at Mt. Lemmon Optical Astronomy Observatory in Arizona.

We use the optical and X-ray afterglow data to explore the nature of this event. Our observations are reported in Section 2. A joint optical and X-ray data analysis is present in Section 3. Conclusions and discussion are present in Section 4. The notation $f_\nu \propto t^{-\alpha} \nu^{-\beta}$ is used throughout the paper, where f_ν is the spectral flux density at the frequency ν .

2 OBSERVATIONS

GRB 090416 was detected by *Swift* Burst Alert Telescope (BAT) at 12:48:47 UT on 2009 April 26 (Cummings et al. 2009). Its duration is $T_{90} = 1.28 \pm 0.09$ sec in 15-350 KeV. *Swift* X-Ray Telescope (XRT) began to observe the burst since 84.6 sec after the GRB trigger. At 89 sec after the trigger, *Swift* UltraViolet Optical Telescope (UVOT) began to observe the burst and reported an optical counterpart with a brightness of about 17.5 mag in the white band. The optical afterglow was confirmed by the Xinglong TNT telescope (Xin et al. 2009) and other follow-up observations (e.g. Im et al. 2009). A redshift of 2.609 was determined by Levesque et al. (2009c) using the Keck telescope, which was confirmed by the ESO VLT Spectrograph observation (Thoene et al. 2009). The time-integrated γ -ray spectrum is well fit by a power-law with a photon index of 1.93 (Sato et al. 2009), which roughly corresponds to an estimated spectral peak energy (in the observer frame) $E_{p,obs} \sim 45$ keV using an empirical relation between E_p and the power-law photon index of the BAT spectrum (Zhang et al. 2007a; Sakamoto et al. 2009).

2.1 Optical Observation and Data Reduction

We carried out a follow-up observation campaign of GRB 090426 using the TNT (0.8-m Tsinghua University - National Astronomical Observatory of China Telescope) at Xinglong Observatory, under the framework of East-Asia GRB Follow-up Observation Network (EAFON, Urata et al. 2003; 2005). TNT is equipped with a PI 1300 \times 1340 CCD and filters in the standard Johnson Bessel system. Its field of view is 11.4 \times 11.4 arcmin, yielding a 0.5 arcsec pixel scale. A custom-designed automation system has been developed for the GRB follow-up observations (Zheng et al. 2008).

The observation of the optical transient (OT) of GRB 090426 was carried out with TNT at 86 seconds post the *Swift*/BAT trigger, which is slightly earlier than the beginning observation of XRT and UVOT on-board *Swift*. A new fading source was discovered and confirmed as the OT of the burst (Xin et al. 2009). The coordinates of the OT are consistent with that of UVOT (Cummings et al. 2009). The W (white), R and V -band images were obtained in 86–519 seconds, 570–1513 seconds, and 1907–10748 seconds post the GRB trigger, respectively.

The 1-m telescope (Han et al. 2005) is located at Mt. Lemmon Optical Astronomy Observatory LOAO in Arizona operated by the Korea Astronomy Space Science Institute. The observation of GRB 090426 was carried out at about 16.3 hours after the burst ($t \sim 60$ ks) in the R filter. The OT was not detected and only upper limits were obtained.

Data reduction was carried out following the stan-

standard routine in IRAF¹ package, including bias and flat-field corrections. Dark correction was not performed since the temperature of our CCD was cooled down to -110°C . Point spread function (PSF) photometry was applied via the DAOPHOT task in the IRAF package to obtain the instrumental magnitudes. During the reduction, some frames were combined in order to increase the signal-to-noise ratio (S/N). In the calibration and analysis, the white band was treated as the R band (Xin et al. 2010). Absolute calibration was performed using the Sloan Digital Sky Survey (SDSS, Adelman-McCarthy et al. 2008), with conversion of SDSS to Johnson-Cousins system². The data of GRB 090426 obtained by TNT and LOAO are reported in Table. 1.

2.2 Swift/XRT X-ray Afterglow Data Reduction

The *Swift*/XRT lightcurve and spectrum are extracted from the UK Swift Science Data Centre at the University of Leicester (Evans et al. 2009)³. We fit the X-ray spectrum with the *Xspec* package. The time-integrated X-ray spectrum is well fit by an absorbed power-law model, with a photon power-law index $\Gamma = 2.00 \pm 0.06$ from the PC mode data. No significant host N_H excess over the Galactic value is detected.

3 OPTICAL AND X-RAY AFTERGLOW JOINT ANALYSIS

3.1 Temporal Analysis

With the X-ray spectral index ($\beta_X = 1.00 \pm 0.06$), we first derive the 1 keV lightcurve from the XRT data. It is shown in Fig. 1. Next, we convert the extinction-corrected magnitudes of the optical afterglow into energy fluxes. Levesque et al. (2010a) reported $A_V \sim 0.4$ for the GRB host galaxy, and the extinction by the MilkyWay Galaxy in the burst direction is $E_{B-V} = 0.017$ (Schlegel et al.1998). For the host galaxy, the transformation from A_V to A_R is nearly independent of any known type of extinction laws (MW, LMC, SMC), and we take $A_R \sim 0.32$ for the host galaxy. The Milky Way extinction corresponds to $A_R = 0.046$ and $A_V = 0.057$. After extinction corrections, we find that the νF_ν fluxes in both the optical and the X-ray bands are almost the same. This indicates a flat νF_ν spectrum from the optical to the X-ray bands, i.e., $\beta_{OX} \sim 1.0$. This is consistent with the observed X-ray spectral index. This flat νF_ν spectrum also means that we do not need to calibrate the observed optical fluxes to a given band. The extinction-corrected optical energy flux lightcurve is also shown in Fig. 1.

As shown in Fig. 1, the afterglow lightcurves in the optical and X-ray bands trace with each other, suggesting that not only they are of the similar (external shock) origin, but also they belong to the same spectral regime. At the early epoch $t < 2200$ seconds post the GRB trigger, the optical

Table 1. Optical Afterglow Photometry Log of GRB 090426. The reference time T_0 is *Swift* BAT burst trigger time. All Data are not corrected for the Galactic extinction (which is $E_{B-V} = 0.017$, Schlegel et al.1998). ‘‘Merr’’ means the uncertainty of magnitude.

T-T0(mid) sec	Exposure sec	Mag	Merr	Filter	Telescope
86	20.0	16.44	0.03	W	TNT
109	20.0	16.50	0.03	W	TNT
133	20.0	16.59	0.03	W	TNT
155	20.0	16.66	0.03	W	TNT
178	20.0	16.76	0.03	W	TNT
201	20.0	16.88	0.04	W	TNT
223	20.0	17.01	0.04	W	TNT
246	20.0	17.01	0.04	W	TNT
269	20.0	17.07	0.04	W	TNT
292	20.0	17.09	0.04	W	TNT
314	20.0	17.22	0.04	W	TNT
337	20.0	17.30	0.05	W	TNT
360	20.0	17.31	0.05	W	TNT
382	20.0	17.44	0.05	W	TNT
405	20.0	17.50	0.06	W	TNT
428	20.0	17.56	0.06	W	TNT
451	20.0	17.69	0.06	W	TNT
473	20.0	17.63	0.06	W	TNT
496	20.0	17.80	0.06	W	TNT
519	20.0	17.89	0.06	W	TNT
570	60.0	17.93	0.06	R	TNT
649	60.0	18.12	0.07	R	TNT
728	60.0	18.30	0.07	R	TNT
807	60.0	18.38	0.08	R	TNT
885	60.0	18.46	0.09	R	TNT
964	60.0	18.72	0.08	R	TNT
1042	60.0	18.71	0.08	R	TNT
1121	60.0	18.78	0.11	R	TNT
1199	60.0	18.85	0.11	R	TNT
1278	60.0	19.01	0.11	R	TNT
1356	60.0	19.04	0.12	R	TNT
1435	60.0	19.12	0.12	R	TNT
1513	60.0	19.06	0.12	R	TNT
1907	300×2	19.72	0.12	V	TNT
2542	300×2	20.04	0.12	V	TNT
3178	300×2	20.10	0.12	V	TNT
3813	300×2	20.05	0.12	V	TNT
4448	300×2	20.17	0.12	V	TNT
5084	300×2	20.19	0.14	V	TNT
5878	300×3	20.30	0.14	V	TNT
7048	600×2	20.47	0.16	V	TNT
8282	600×2	20.69	0.17	V	TNT
9515	600×2	20.65	0.17	V	TNT
10748	600×2	20.71	0.18	V	TNT
58591	180×10	>21.67		R	LOAO

Table 2. Optical lightcurve fits with a smooth broken power-law model for two epoches.

Interval	F_0^*	t_p (s)	α_1	α_2
86-2200s	3.74±0.32	227±27	0.26±0.07	1.22±0.04
> 2200 s	1.77±0.67	7123±3620	0.19±0.41	~ 1.22

*In units of $\times 10^{-12}$ erg cm^{-2} s^{-1} .

¹ IRAF is distributed by NOAO, which is operated by AURA, Inc., under cooperative agreement with NSF.
² <http://www.sdss.org/dr6/algorithms/sdssUBVRITransform.html>
³ <http://www.swift.ac.uk/results.shtml>

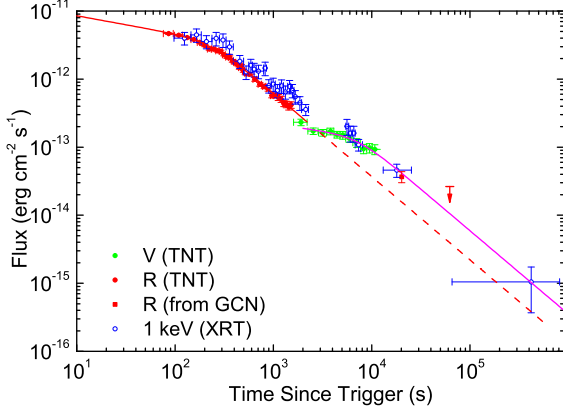


Figure 1. The extinction-corrected optical light curve of GRB 090426 (solid dots) and the best fit with a smooth broken power-law model (solid line) for two epoches before and after 2200 seconds post the GRB trigger. The R -band data observed by Rumyantsev et al. (2009) is marked with squares. The XRT lightcurve (open dots) is also shown for comparison.

and X-ray afterglow lightcurves show a smooth shallow-to-normal transition in the decaying behavior, with small flickerings in the X-ray band. In the time interval 2200 – 5500 seconds, the brightness of the OT kept almost a constant. It then faded again at $t > 5500$ seconds. The OT was also detected by Rumyantsev et al. (2009) at 0.2342 days (20200 seconds) post the GRB trigger. It faded down to $R = 21.3 \pm 0.2$, indicating a decay slope of ~ 1.2 in the time interval of $t > 5500$ seconds. Due to the orbital constraints of the *Swift* satellite, there is no XRT observation in the time interval [2200, 5500] seconds when the optical lightcurve features a plateau. The fading behavior of X-rays in the time interval [5500, 7700] seconds is similar to that of the optical afterglow. At $t \sim 0.2342$ day, the detected X-ray behavior is also consistent with that of the optical emission. These results suggest that the temporal behavior of both optical and X-ray afterglows could be the same. We thus perform a temporal analysis on the well-sampled optical lightcurve only. The optical lightcurves in the time intervals both before and after 2200 seconds can be well fit with a smooth broken power-law,

$$F = F_0 \left[\left(\frac{t}{t_b} \right)^{\omega\alpha_1} + \left(\frac{t}{t_b} \right)^{\omega\alpha_2} \right]^{-1/\omega}. \quad (1)$$

Our best-fit parameters are summarized in Table. 2. We find that the decay slopes post the two breaks are similar, with a value ~ 1.22 . The late time X-ray data at $\sim 4 \times 10^5$ s is also consistent with the predicted behavior of such a decay slope in the X-ray band.

3.2 Data Confronted with the Forward Shock Models

As shown above, the temporal behaviors of the optical and X-ray data are consistent with being achromatic, and the decay slopes after the two breaks observed in the optical

lightcurve are well consistent with the prediction of the forward shock models. The fact $\alpha_o = \alpha_x$ suggests that the emissions in both bands are consistent with the forward shock model in the same spectral regime (see also Urata et al. (2007) for a more general discussion of the $\alpha_o - \alpha_x$ relation for the forward shock models). We find no spectral evolution across the two breaks from the X-ray data. The derived β_X are 1.09 ± 0.15 and 1.03 ± 0.10 , respectively, for the integrated X-ray spectra at $t < 2200$ s and $t > 2200$ s. Inspecting the spectral index β_X and the temporal decay index α_X in the normal decay segment, one finds good agreement between data and the forward shock model closure relation in the spectral regime $\nu > \max(\nu_m, \nu_c)$, i.e. $\alpha = (3\beta_X - 1)/2 = 1.14 \pm 0.23$, where ν_m and ν_c are the typical and cooling frequencies of synchrotron radiation, respectively. Since both optical and X-ray emissions are consistent with the forward shock origin in the normal decay phase, one can naturally attribute the two shallow decay segments to two epochs of energy injection into the blastwave (e.g., Dai & Lu 1998; Zhang & Meszaros 2001; Zhang et al. 2006; Liang et al. 2007).

3.3 Constraints on the Burst Environment

The circumburst environment is critical to understand the nature of a GRB. In the literature, usually two types of medium are discussed, namely, a constant density medium relevant for interstellar medium (ISM) or a stratified stellar wind with a density profile $n \propto r^{-2}$. For the spectral regime identified for GRB 090426, i.e. $\nu > \max(\nu_m, \nu_c)$, unfortunately the observed flux does not depend on the medium density. Consequently, one can not distinguish the two types of medium. However, since a wind model would undoubtedly point towards a massive star progenitor, we only focus on the constant density case. According to the analysis in section 3.2, ν_c should be below the optical band at the very early epoch. This would give an interesting constraint on the medium density.

In the constant density case, the typical synchrotron emission frequency, the cooling frequency and the peak spectral flux density are (Sari et al. 1998; coefficients taken from Yost et al. 2003; Zhang et al. 2007b):

$$\nu_m = 3.3 \times 10^{12} \text{ Hz} \left(\frac{p-2}{p-1} \right)^2 (1+z)^{1/2} \epsilon_{B,-2}^{1/2} \epsilon_{e,-1}^2 E_{K,52}^{1/2} t_d^{-3/2} \quad (2)$$

$$\nu_c = 6.3 \times 10^{15} \text{ Hz} (1+z)^{-1/2} (1+Y)^{-2} \epsilon_{B,-2}^{-3/2} E_{K,52}^{-1/2} n^{-1} t_d^{-1/2} \quad (3)$$

$$F_{\nu,\max} = 1.6 \text{ mJy} (1+z) D_{28}^{-2} \epsilon_{B,-2}^{1/2} E_{K,52} n^{1/2} \quad (4)$$

where D is the luminosity distance in units of 10^{28} cm, f_p is a function of p ($f_p \sim 1$ for $p = 2$, Zhang et al. 2007b), and t_d is the observer's time in unit of days. The convention $Q_n = Q/10^n$ is adopted in cgs units. The Inverse Compton scattering parameter

$$Y = [-1 + (1 + 4\eta_1 \eta_2 \epsilon_e / \epsilon_B)^{1/2}] / 2, \quad (5)$$

where $\eta_1 = \min[1, (\nu_c / \nu_m)^{(2-p)/2}] \sim 1$ for $p \sim 2.0$ (Sari & Esin 2001), and $\eta_2 \leq 1$ is a correction factor introduced by the Klein-Nishina effect. We take $\eta_2 = 1$ in our analysis, so

that the R -band energy flux reads

$$\begin{aligned}\nu_R F_{\nu_R} &= F_{\nu, \max} \nu_c^{1/2} \nu_m^{(p-1)/2} \nu_R^{(2-p)/2} \\ &= 2.67 \times 10^{-11} f_p \text{ ergs s}^{-1} \text{ cm}^{-2} D_{28}^{-2} (1+z)^{(p+2)/4} \\ &\times (1+Y)^{-1} \epsilon_{B,-2}^{(p-2)/4} \epsilon_{e,-1}^{p-1} E_{K,52}^{(p+2)/4} t_d^{(2-3p)/4} \nu_R^{(2-p)/2} \quad (6)\end{aligned}$$

where

$$f_p = \left[7.45 \times 10^{-3} \left(\frac{p-2}{p-1} \right)^2 \right]^{(p-1)/2}. \quad (7)$$

Since $p = 2\beta = 2.18 \pm 0.30$, we have $f_p = 6.04 \times 10^{-3}$. One can then derive E_K using the data at any time t_d (Zhang et al. 2007b):

$$\begin{aligned}E_{K,52} &= \left[\frac{\nu_R F_{\nu_R}}{1.61 \times 10^{-13} \text{ ergs s}^{-1} \text{ cm}^{-2}} \right]^{4/(p+2)} \\ &\times D_{28}^{8/(p+2)} (1+z)^{-1} t_d^{(3p-2)/(p+2)} \\ &\times (1+Y)^{4/(p+2)} \epsilon_{B,-2}^{(2-p)/(p+2)} \\ &\times \epsilon_{e,-1}^{4(1-p)/(p+2)} \nu_R^{2(p-2)/(p+2)}. \quad (8)\end{aligned}$$

The analysis above is valid for $p > 2$. From the X-ray data, we find the p is slightly larger than 2. In order to make a rough estimate, we take $p \sim 2$ to simplify Eq. 8 as

$$E_{k,52} = \frac{\nu_R F_{\nu_R}}{1.61 \times 10^{-13} \text{ ergs s}^{-1} \text{ cm}^{-2}} \frac{t_d}{1+z} \epsilon_{e,-1}^{-1} (1+Y) D_{L,28}^2. \quad (9)$$

The cooling frequency ν_c is given by

$$\begin{aligned}\nu_c &= 6.3 \times 10^{15} \text{ Hz} \left(\frac{\nu_R F_{\nu_R}}{1.61 \times 10^{-13} \text{ ergs s}^{-1} \text{ cm}^{-2}} \right)^{-1/2} \\ &\times (1+Y)^{-5/2} \epsilon_{B,-2}^{-3/2} \epsilon_{e,-1}^{1/2} n^{-1} t_d^{-1} D_{28}^{-1}. \quad (10)\end{aligned}$$

At $t \sim 100$ seconds, one has $\nu_R F_{\nu_R} = 4.42 \times 10^{-12} \text{ erg cm}^{-2} \text{ s}^{-1}$, so that

$$\nu_c = 1.57 \times 10^{17} \text{ Hz} (1+Y)^{-5/2} \epsilon_{B,-2}^{-3/2} \epsilon_{e,-1}^{1/2} n^{-1}. \quad (11)$$

The requirement of $\nu_R > \nu_c$ at $t \sim 100$ seconds then gives

$$n > 354s(\epsilon_e, \epsilon_B), \quad (12)$$

where $s(\epsilon_e, \epsilon_B) = \epsilon_{B,-2}^{-3/2} \epsilon_{e,-1}^{1/2} (1+Y)^{-5/2}$. This already points towards a large medium density. Noticing that s would decrease when ϵ_B increases, we consider an extreme case of energy equipartition among radiating electrons, magnetic field and baryons, i.e., $\epsilon_e = 1/3$, $\epsilon_B = 1/3$. In this case, we still get $n > 11.2 \text{ cm}^{-3}$. Such a dense medium is inconsistent with the naive expectation of a compact star merger progenitor, which tend to occur in low-density medium as the compact binary escapes from the star forming region due to the natal kicks during the births of the two neutron stars. The high density, on the other hand, is consistent with that expected for a massive star that was born in a high density star forming region such as a molecular cloud (e.g. Chevalier et al. 2004).

Recall that a stellar wind medium also suggests a massive star connection, we therefore conclude that GRB 090426 is a Type II GRB, i.e., its progenitor is most likely a massive star.

4 DISCUSSION AND CONCLUSIONS

We have presented the early optical afterglow observations of GRB 090426 with TNT and LOAO. Our well-sampled optical afterglow lightcurve from ~ 90 seconds to $\sim 10^4$ seconds post the GRB trigger seems to exhibit two energy injection phases that ended at ~ 230 seconds and ~ 7100 seconds, respectively. The temporal feature of the observed X-rays is consistent with the optical emission. We show that both the optical and X-ray afterglows are consistent with the forward shock model in the spectral regime $\nu > \max(\nu_m, \nu_c)$. Although the medium type (ISM vs. wind) cannot be distinguished, we can make a case of the massive star (Type II) origin of the GRB. For a constant density medium, the required medium density is found very high (Eq.[12]), inconsistent with the expectation of a compact star merger (Type I) progenitor. A massive star progenitor forming in a high-density star forming region (e.g. molecular cloud) is consistent with the data. If the circumburst medium is a stellar wind, then it also directly points towards a massive star progenitor. We therefore conclude that the afterglow data of the short GRB 09046 strongly suggests that it is a Type II GRB.

GRB 090426 is of great interest because of its short duration ($T_{90} \sim 0.33$ seconds in the burst frame) and high redshift ($z = 2.609$). Its redshift significantly exceeds the previous spectroscopically confirmed high redshifts of short GRBs, e.g. GRB 070714B ($z = 0.904$, Graham et al. 2009), GRB 051121A ($z = 0.546$, Soderberg et al. 2006b), GRB 070429 ($z = 0.902$, Cenko et al. 2008) and GRB 090510 ($z = 0.903$, Rau et al. 2009). Its host galaxy is a blue, luminous, and star-forming galaxy (Levesque et al. 2010a), similar to the host galaxies of typical Type II GRBs (Levesque et al. 2010b). The spectral energy correlation is also consistent with being a Type II GRB. Here we present a third argument in favor of its Type II origin, based on early afterglow observation and modeling. It is interesting to note that with the new classification method proposed by Lv et al. (2010), GRB 090426 is well grouped into Type II GRBs, in contrast to other short GRBs such as GRB 051221 and GRB 070714B. We also noted that GRB 090426 shares some similar properties with two other Type II bursts, GRB 040924 and GRB 050416A. The first was a short-duration (1.2-1.5 sec), soft spectrum (Huang et al. 2005) and a SN 1998bw-like supernova-associated burst (Soderberg et al. 2006a; Wiersema et al. 2008). The second burst also exhibited a soft spectrum and a short duration in the rest frame ($T_{90} = 2.4s$, $z = 0.6528$), which is associated with a SN 1998bw-like supernova (Soderberg et al. 2007), and is located in a circumburst medium with a large density variation.

Finally, our result reinforces the suggestion of Zhang et al. (2009) that burst duration alone cannot be used to judge the physical nature of a GRB, and that some short GRBs can be of the Type II origin. Multi-wavelength observational campaigns are essential to unveil the physical nature of GRBs.

5 ACKNOWLEDGEMENT

The authors thank the anonymous referee for helpful suggestions and comments, and Massimiliano De Pasquale for

correcting an error in the early version. This work made use of data supplied by the UK *Swift* Science Data Center at the University of Leicester. It is partially supported by the National Natural Science Foundation of China under grants No. 10673014, 10803008, 10873002, and the National Basic Research Program ("973" Program) of China under Grant 2009CB824800. It is also partly supported by grants NSC 98-2112-M-008-003-MY3 (Y.U.), and by NASA NNX09AT66G, NNX10AD48G, and NSF AST-0908362 (B.Z.). E. W. L. also acknowledges the support from the Guangxi SHI-BAI-QIAN project (Grant 2007201), the Guangxi Science Foundation (2010GXNSFC013011) the program for 100 Young and Middle-aged Disciplinary Leaders in Guangxi Higher Education Institutions, and the research foundation of Guangxi University (M30520). MI and YS are supported by the Korea Science and Engineering Foundation (KOSEF) grant No. 2009-0063616, funded by the Korean government (MEST). K.Y.H. was supported by NSC-99-2112-M-001-002-MY3.

REFERENCES

- Adelman-McCarthy J. K., et al., 2008, *ApJS*, 175, 297
 Antonelli L. A., et al., 2009, *A&A*, 507, L45
 Barthelmy S. D., et al., 2005, *Natur*, 438, 994
 Belczynski K., Holz D. E., Fryer C. L., Berger E., Hartmann D. H., O'Shea B., 2010, *ApJ*, 708, 117
 Berger E., et al., 2005, *ApJ*, 634, 501
 Berger E., et al., 2007, *ApJ*, 664, 1000
 Campana S., et al., 2006, *Natur*, 442, 1008
 Cenko S. B., et al., 2008, *arXiv*, arXiv:0802.0874
 Chevalier R. A., Li Z.-Y., Fransson C., 2004, *ApJ*, 606, 369
 Cummings J. R., et al., 2009, *GCN*, 9254, 1
 Dai Z. G., Lu T., 1998, *A&A*, 333, L87
 Eichler D., Livio M., Piran T., Schramm D. N., 1989, *Natur*, 340, 126
 Evans P. A., et al., 2009, *MNRAS*, 397, 1177
 Fong W., Berger E., Fox D. B., 2010, *ApJ*, 708, 9
 Fox D. B., et al., 2005, *Natur*, 437, 845
 Fynbo J. P. U., et al., 2006, *Natur*, 444, 1047
 Gal-Yam A., et al., 2006, *Natur*, 444, 1053
 Galama T. J., et al., 1998, *Natur*, 395, 670
 Gehrels N., et al., 2005, *Natur*, 437, 851
 Gehrels N., et al., 2006, *Natur*, 444, 1044
 Graham J. F., et al., 2009, *ApJ*, 698, 1620
 Greiner J., et al., 2009, *ApJ*, 693, 1610
 Han W., et al., 2005, *PASJ*, 57, 821
 Hjorth J., et al., 2003, *Natur*, 423, 847
 Huang K. Y., et al., 2005, *ApJ*, 628, L93
 Im M., Jeon Y., Lee I., Jeon Y.-B., Urata Y., 2009, *GCN*, 9276, 1
 Kann D. A., et al., 2007, *arXiv*, arXiv:0712.2186
 Kann D. A., et al., 2008, *arXiv*, arXiv:0804.1959
 Kouveliotou C., Meegan C. A., Fishman G. J., Bhat N. P., Briggs M. S., Koshut T. M., Paciesas W. S., Pendleton G. N., 1993, *ApJ*, 413, L101
 Levan A. J., et al., 2006, *ApJ*, 648, L9
 Levan A. J., et al., 2007, *MNRAS*, 378, 1439
 Levesque E. M., et al., 2010a, *MNRAS*, 401, 963
 Levesque E. M., Berger E., Kewley L. J., Bagley M. M., 2010b, *AJ*, 139, 694
 Levesque E., Chornock R., Kewley L., Bloom J. S., Prochaska J. X., Perley D. A., Cenko S. B., Modjaz M., 2009c, *GCN*, 9264, 1
 Liang E., Zhang B., 2005, *ApJ*, 633, 611
 Liang E.-W., Zhang B.-B., Zhang B., 2007, *ApJ*, 670, 565
 Lin L., Liang E.-W., Zhang B.-B., Zhang S. N., 2008, *AIPC*, 1065, 39
 Lin L., Wei L. E., Shuang Nan Z., 2009, *arXiv:0906.3057*
 Lü H., Liang E., Zhang B., Zhang B., 2010, *arXiv:1001.0598*
 McGlynn S., Foley S., McBreen S., Hanlon L., O'Connor R., Carrillo A. M., McBreen B., 2008, *A&A*, 486, 405
 Nakar E., 2007, *PhR*, 442, 166
 Narayan R., Paczynski B., Piran T., 1992, *ApJ*, 395, L83
 Norris J. P., Bonnell J. T., 2006, *ApJ*, 643, 266
 Paczynski B., 1998, *ApJ*, 494, L45
 Perley D. A., et al., 2009, *ApJ*, 696, 1871
 Piran T., 2004, *RvMP*, 76, 1143
 Rau A., McBreen S., Kruehler T., 2009, *GCN*, 9353, 1
 Rumyantsev V., Antoniuik K., Pozanenko A., 2009, *GCN*, 9320, 1
 Sakamoto T., et al., 2009, *ApJ*, 693, 922
 Salvaterra R., et al., 2009, *Natur*, 461, 1258
 Sari R., Piran T., Narayan R., 1998, *ApJ*, 497, L17
 Sari R., Esin A. A., 2001, *ApJ*, 548, 787
 Sato G., et al., 2009, *GCN*, 9263, 1
 Schlegel D. J., Finkbeiner D. P., Davis M., 1998, *ApJ*, 500, 525
 Soderberg A. M., et al., 2004, *Natur*, 430, 648
 Soderberg A. M., et al., 2006a, *ApJ*, 636, 391
 Soderberg A. M., et al., 2006b, *ApJ*, 650, 261
 Soderberg A. M., et al., 2007, *ApJ*, 661, 982
 Tanvir N. R., et al., 2009, *Natur*, 461, 1254
 Thoene C. C., et al., 2009, *GCN*, 9269, 1
 Urata Y., et al., 2003, *ApJ*, 595, L21
 Urata Y., et al., 2005, *NCimC*, 28, 775
 Urata Y., et al., 2007, *ApJ*, 668, L95
 Villaseñor J. S., et al., 2005, *Natur*, 437, 855
 Wiersema K., et al., 2008, *A&A*, 481, 319
 Woosley S. E., 1993, *ApJ*, 405, 273
 Woosley S. E., Bloom J. S., 2006, *ARA&A*, 44, 507
 Xin L. P., Zheng W. K., Qiu Y. L., Wei J. Y., Wang J., Deng J. S., Urata Y., Hu J. Y., 2009, *GCN*, 9255, 1
 Xin L. P., et al., 2010, *MNRAS*, 401, 2005
 Yost S. A., Harrison F. A., Sari R., Frail D. A., 2003, *ApJ*, 597, 459
 Zhang B., Mészáros P., 2001, *ApJ*, 552, L35
 Zhang B., Mészáros P., 2004, *IJMPA*, 19, 2385
 Zhang B., Fan Y. Z., Dyks J., Kobayashi S., Mészáros P., Burrows D. N., Nousek J. A., Gehrels N., 2006, *ApJ*, 642, 354
 Zhang B., Zhang B.-B., Liang E.-W., Gehrels N., Burrows D. N., Mészáros P., 2007a, *ApJ*, 655, L25
 Zhang B., et al., 2007b, *ApJ*, 655, 989
 Zhang B., et al., 2009, *ApJ*, 703, 1696
 Zheng W.-K., et al., 2008, *ChJAA*, 8, 693